A CS SURVEY OF LOW-MASS CORES AND COMPARISON WITH NH₃ OBSERVATIONS

SHUDONG ZHOU, YUEFANG WU,[1] AND NEAL J. EVANS II
Department of Astronomy and Electrical Engineering Laboratory, University of Texas at Austin

GARY A. FULLER
Astronomy Department and Radio Astronomy Laboratory, University of California, Berkeley

AND

PHILIP C. MYERS
Harvard-Smithsonian Center for Astrophysics

ABSTRACT

We present CS observations with resolutions of 1′–2′ of low-mass molecular cloud cores; the results are compared with those of previous NH₃ observations. Our analysis shows that CS and NH₃ emission give somewhat different results for the properties of the cores. In comparison with the NH₃ emission, the CS emission comes from a larger region and has a larger velocity dispersion. The mass and density derived from the CS data are also larger by 1–2 orders of magnitude than those derived from the NH₃ data. On the other hand, both CS and NH₃ emission lines are at the same velocity, and statistically both CS and NH₃ lines have wider line widths toward cores with associated *IRAS* sources. This seems to indicate that CS and NH₃ are probing regions closely related to star formation in the dense cores in spite of some differences in their properties.

We have considered several possibilities that might cause the differences in the line widths of CS and NH₃ emissions, such as the effects due to the difference in optical depth, the different sizes of the emission regions, and chemical differentiation.

Subject heading: interstellar: molecules

I. INTRODUCTION

Based on molecular line and infrared observations, small dense cores have been found to be regions of low-mass star formation (Myers and Benson 1983; Beichman *et al.* 1986; Myers *et al.* 1987; Benson and Myers 1989). In an ammonia survey of regions of high visual extinction, Myers and Benson (1983) have found a number of small cores, 0.1 pc in size, with densities $\sim 10^4$ cm^{-3}. The positions of the dense cores are found to correlate well with emission-line stars, which suggests that they are closely related to newly formed stars. A comparison with the *IRAS* survey indicates that these dense cores may contain protostars. In a statistical study, Beichman *et al.* (1986) have found that half the sample dense cores they chose have *IRAS* sources associated with them, and more than half the *IRAS* sources have no visible counterparts. These *IRAS* sources inside the dense cores without visible counterparts are potential protostars. Based on statistical arguments, over one-third of the *IRAS* sources could be protostars (Beichman *et al.* 1986).

One notable feature of the dense cores is their extremely narrow ammonia lines ($\Delta V \sim 0.3$ km s^{-1}). Myers and Benson (1983) analyzed the ammonia line profiles and found that they could be explained by thermal motion plus either a subsonic microturbulence or an early collapse with an age less than 10^5 yr. In either case, thermal motion dominates the line broadening. A natural consequence of the dominance of thermal motion is that molecular species having similar nonthermal motions, but greater molecular mass m than ammonia, should show a narrower line width since $\Delta V_{th} \propto (T/m)^{1/2}$. The nature of line broadening in the dense cores is important to our

understanding of how stars form in cores, since the random component reveals the internal pressure which resists collapse, and the systematic component can reveal the relative importance of the gravitational, rotational, and outflow motions in the star-forming process.

By observing lines of heavier molecules which trace similar density ranges as does the NH₃(1, 1) line, one can test whether the line broadening within dense cores is truly dominated by thermal motion. To understand further the properties of the dense cores, we have observed the CS($J = 2 \rightarrow 1$), ($3 \rightarrow 2$), and ($5 \rightarrow 4$) lines in a sample of objects consisting partly of cores associated with *IRAS* sources and partly of cores not associated with *IRAS* sources. We will derive density structures from our CS observations and compare them with previous NH₃ observations. We will pay special attention to the line widths of both molecules. In addition, the differences in general physical conditions between cores with and without embedded infrared sources should give us some clues to how the cores evolve and eventually form stars.

In this paper, we concentrate on the physical conditions traced by CS and the comparison with NH₃. A list of references to other related observations is given in Table 1. Our main conclusions are the following. CS emission is detected in 25 out of 27 dense cores; typical size, line width, and density of the CS emission regions are 0.3 pc, 0.6 km s^{-1}, and 10^5 cm^{-3}, respectively. Half of the dense cores have associated *IRAS* sources where the CS lines show enhanced widths. Comparison with previous NH₃ surveys show that CS lines are wider than NH₃ lines and are clearly not dominated by thermal broadening. While other explanations are possible, chemical differentiation is suspected. The physical conditions traced by CS indicate that most of the dense cores are unstable.

---

[1] Visiting Scholar from Beijing University, China.

TABLE 1
Source Coordinates

Source Name	R.A.	Decl.	V_{lsr} (km s^{-1})	Associated *IRAS* Source	References
B5	03^{h}44^{m}33^{s}5	32°42′30″	10.1	03455+3242	a, b, c
L1489	04 01 45.0	26 11 33	6.8	04016+2610	a, b, c, d
L1498	04 07 50.0	25 02 13	7.8	...	c, d
L1495	04 11 06.0	28 01 52	6.9	...	c, d
L1400 G	04 21 05.1	54 52 20	3.4	...	d
B217	04 24 42.0	26 11 12	7.0	...	d
TMC 2	04 29 43.0	24 18 54	6.3	...	c, d
L1535	04 32 33.2	24 03 00	5.9	04325+2402	e
TMC 1A	04 36 35.4	25 35 56	5.4	04365+2535	a, c, f
TMC 1	04 38 39.0	25 36 18	5.8	..	a, c, e
L1512	05 00 54.5	32 39 00	7.1	...	c, d
L1582 A	05 29 11.9	12 28 20	10.1	2 μm source	a, b, c, f
L 1582 B	05 29 32.0	12 47 31	10.3	05295+1247	a, c, f
B35	05 41 45.3	09 07 40	11.7	05417+0907	a, c, f
L134 A	15 50 58.1	−04 26 36	2.7	...	d
L183	15 51 35.0	−02 40 54	2.4	...	c, d
L1696 A	16 25 29.0	−24 11 32	3.4	...	c, d
L1709	16 28 34.0	−23 55 04	2.6	...	c, f
L43 B	16 31 42.0	−15 41 00	0.6	16316−1540	a, c, d
L255	16 44 14.1	−09 30 02	3.5	16442−0930	a, c, f
L234 A	16 45 20.0	−10 46 33	2.8	...	d
L63	16 47 21.0	−18 01 00	5.9	...	d
L1152	20 35 17.0	67 43 15	2.4	20353+6742	a, c, e
L1174	20 59 46.0	68 01 04	2.7	20597+6800	a, c, e
L1172	21 01 48.0	67 42 12	2.7	21017+6742	a, c, e
L1251	22 29 03.2	74 58 51	−4.0	22290+7458	f
L1262 A	23 23 32.0	74 01 45	4.0	23238+7401	a, b, c, d

References.—(a) Beichman *et al.* 1986; (b) Benson *et al.* 1984; (c) Myers *et al.* 1983; (d) Myers and Benson 1983; (e) Ungerechts *et al.* 1982; (f) Benson 1983.

II. OBSERVATIONS

The CS observations were made partly at the NRAO[2] 12 m telescope at Kitt Peak and partly at the 4.9 m telescope of the Millimeter Wave Observatory[3] (MWO) near Fort Davis, Texas. For both telescopes, we consistently adopt the calibration scheme described in Kutner and Ulich (1981). T_A^* is the antenna temperature corrected for atmospheric attenuation and rear spillover and scattering. The correction for the coupling of the forward beam to the source is described by the product of two efficiencies: η_{fss} and η_c. The quantity η_{fss} is the fraction of power falling into the forward hemisphere which is within a solid angle, including the main beam, with an angular size of the Moon; η_c is the coupling efficiency between the antenna beam shape within the size of the Moon and the brightness distribution of the source.

The observations of the CS($J = 2 \rightarrow 1$) line were made at the NRAO 12 m telescope. We used 800 K for the calibration temperature in order to account for η_{fss}, and 0.87 for the coupling efficiency (η_c) between the antenna main beam and the source brightness distribution (Phil R. Jewell, private communication 1988). The beam size was about 1′ and the velocity resolution was 0.09 km s^{-1}. The details of the observations, including pointing and calibration, are described in Fuller (1988).

The observations of the C^{34}S($J = 3 \rightarrow 2$) line at 144 GHz, CS($J = 3 \rightarrow 2$) line at 147 GHz, and the CS($J = 5 \rightarrow 4$) line at

245 GHz were made at MWO between 1985 December and 1988 January. For the $J = 3 \rightarrow 2$ observations, we used a 2 mm cryogenic receiver with a single sideband receiver temperature of 700–850 K; the system temperature was between 900 K and 2000 K. For the $J = 5 \rightarrow 4$ observations, we used a 1 mm cryogenic receiver with a single sideband receiver temperature of 800–1000 K; the system temperature was between 1200 K and 2500 K. The filterbanks consisted of 128 channels of 62.5 kHz filters, which gave a velocity resolution of 0.13 km s^{-1} for the $J = 3 \rightarrow 2$ lines and 0.08 km s^{-1} for the $J = 5 \rightarrow 4$ line. The FWHM beam sizes of the telescope were 1′6 and 1′1 for the $3 \rightarrow 2$ and $5 \rightarrow 4$ lines, respectively.

The pointing of the MWO telescope was known to vary with the declination of the observed source. We corrected the pointing of the antenna by observing several pointing sources at different declinations, such as Jupiter, the circumstellar shell of IRC +10216, and the molecular cloud, S140. For sources at or below the declination of S140 (63°), the total pointing uncertainty after the correction was within 0′5.

By observing the Moon, we measured η_{fss} to be 0.84 for the $J = 3 \rightarrow 2$ lines and 0.90 for the $J = 5 \rightarrow 4$ line. The quantity η_c is 0.75 for the $J = 3 \rightarrow 2$ lines and 0.84 for the $J = 5 \rightarrow 4$ line, based on a uniform disk source 2′ in radius and a model of the beam obtained through holographic measurements of the MWO dish. We choose 2′ as the source radius because the average extent of the CS emission in the cores we have mapped is about 4′. In the following discussion, we will present our results either in T_A^* or in $T_R (= T_A^*/\eta_{fss} \eta_c)$.

Table 1 lists the position and velocity of every source that we observed in any line. The positions listed there are peak ammonia line positions from Benson (1983), Myers, Linke, and Benson (1983) with the exception of L1535. All the sources are
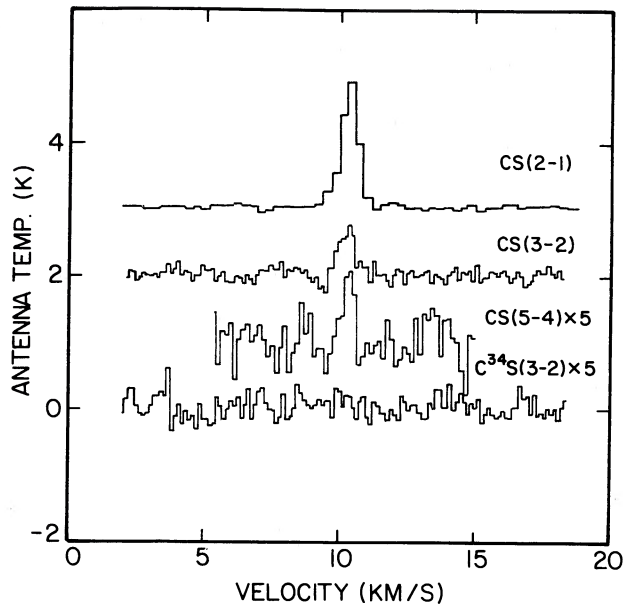
FIG. 1.—Spectra of CS $J = 2 \to 1$, $3 \to 2$, and $5 \to 4$, and $C^{34}S$ $J = 3 \to 2$ toward the (0, 0) position of B5. The scale of the last two spectra are expanded by a factor of 5.

at least observed toward the center position in either the $CS(J = 2 \to 1)$ or the $(3 \to 2)$ line. Fourteen sources have been mapped in the $J = 2 \to 1$ line with 1′ spacing, and seven sources in the $3 \to 2$ line with 2′ spacing (Table 4). Also about seven sources have been observed in the $5 \to 4$ line and another four sources in the $C^{34}S(J = 3 \to 2)$ line (Tables 3 and 5). Typical spectra of all four transitions are shown in Figure 1.

III. PHYSICAL PROPERTIES TRACED BY CS

a) The CS$(2 \to 1)$ and $(3 \to 2)$ lines

We first compare the parameters of the CS$(J = 2 \to 1)$ and $(3 \to 2)$ lines. Table 2 lists the results of Gaussian fits to the spectra of our CS$(2 \to 1$ and $3 \to 2)$ observations toward the center positions listed in Table 1. Column (1) gives the source names. Columns (2), (3), and (4) show the peak radiation temperature (T_R), the FWHM velocity width (ΔV), and the center velocity for the $J = 2 \to 1$ line (V), derived by fitting Gaussians to the observed spectra; all spectra are fitted well with a single Gaussian. Columns (5), (6), and (7) show the same set of data for the $J = 3 \to 2$ line. For sources without detections, we give the 3 σ noise in the spectrum (translated to T_R) in the appropriate column.

The velocity of the two lines agree within 0.1–0.2 km s^{-1}, which is about the same as the spectral resolution used in the observations. A comparison of the line widths for CS $J = 2 \to 1$ with $J = 3 \to 2$ is shown in Figure 2; the typical 1 σ error of the line widths determined from our Gaussian fitting routine is shown in the lower right corner. We see that within a 1.5 σ error, the widths of the two CS lines are equal.

The emission regions of the two lines are also similar, based on the cores we mapped in both the $2 \to 1$ and $3 \to 2$ lines with a few exceptions. Figure 3 shows the half-maximum contours of the peak antenna temperature maps. In B5 (Fig. 3a), the $3 \to 2$ contour deviates from the $2 \to 1$ contour toward the west and southwest, and the peak position of the $3 \to 2$ line is 2′ north of the $2 \to 1$ peak. In L43 B, similar discrepancies occur. We have compared the $2 \to 1$ and $3 \to 2$ maps of these two cores in detail and found that the discrepancies are mainly caused by the larger beam and poor sampling of the $3 \to 2$

TABLE 2

RESULTS OF CS OBSERVATIONS

Source Name (1)	$2 \to 1$ T_R (K) (2)	$2 \to 1$ ΔV (km s^{-1}) (3)	$2 \to 1$ V (km s^{-1}) (4)	$3 \to 2$ T_R (K) (5)	$3 \to 2$ ΔV (km s^{-1}) (6)	$3 \to 2$ V (km s^{-1}) (7)	$\log n(H_2)$ (cm^{-3}) (8)
B5	2.30	0.80	10.3	1.10	0.69	10.1	4.6 ± 0.3
L1489	1.45	0.62	6.9	0.57	0.60	6.8	4.3 ± 0.3
L1498	0.98	0.41	7.9	1.17	0.31	7.8	7.7 ± 0.6
L1495	...	...	...	0.83	0.46	6.9	
L1400 G	0.77	0.79	3.5				
B217	...	...	...	1.02	0.45	7.0	
TMC 2	...	...	...	0.84	0.76	6.3	
L1535	1.56	0.64	5.9	0.73	0.67	5.9	4.3 ± 0.4
TMC 1A	0.68	0.79	6.4	<0.57	...	...	<5.9
TMC 1	...	...	...	1.54	0.57	5.8	
L1512	1.00	0.40	7.2	0.49	0.45	7.1	5.1 ± 0.3
L1582 A	...	...	...	0.62	0.64	10.1	
L1582 B	...	...	...	0.51	1.35	10.3	
B35	1.82	2.31	11.6				
L134 A	0.75	0.46	2.8	0.37	0.62	2.7	5.2 ± 0.3
L183	...	...	...	0.73	0.54	2.4	
L1696 A	...	...	...	1.11	0.68	3.4	
L1709	...	...	...	0.73	0.74	2.6	
L43 B	1.59	0.78	0.7	0.90	0.69	0.6	5.3 ± 0.2
L255	0.71	0.50	3.5	<0.66	...	...	<6.1
L234 A	...	...	...	0.98	0.46	2.8	
L63	...	...	...	0.89	0.39	5.9	
L1152	...	...	...	0.48	0.63	2.4	
L1174	...	...	...	0.57	1.14	2.7	
L1172	...	...	...	0.41	1.42	2.7	
L1251	0.48	1.30	−4.0				
L1262 A	1.00	0.70	4.0	0.67	0.63	4.1	5.7 ± 0.2
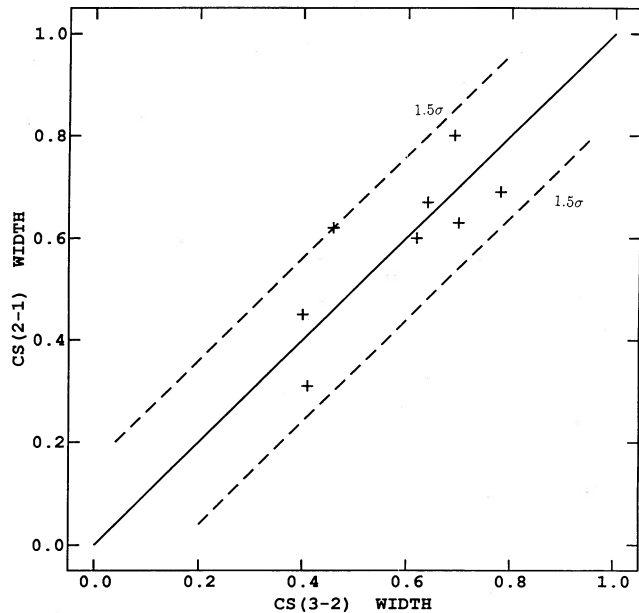
FIG. 2.—Plot of FWHM velocity width of the CS $J = 2 \rightarrow 1$ line vs. that of $J = 3 \rightarrow 2$, in units of km s^{-1}. The solid line indicates where the two widths are the same; the dashed lines indicate the 1.5 σ of measurement errors away from the solid line.

observations. In the case of B5, the $2 \rightarrow 1$ peak is close to the cloud edge where the $3 \rightarrow 2$ beam is so diluted that the $3 \rightarrow 2$ emission does not peak up there. In addition, the sampling toward the west and southwest was very poor, which accounts for the deviation in the half-maximum contour. Overall, if we take the $2 \rightarrow 1$ map and convolve it with the $3 \rightarrow 2$ beam and take into account the undersampling, we would get a map very close to the $3 \rightarrow 2$ map. In L1262 A, it seems the $3 \rightarrow 2$ emission is shifted from the $2 \rightarrow 1$ map by 1' to the SW. Since L1262 A has a declination of 74°, the pointing uncertainties of the NRAO 12 m and the MWO 5 m telescope may account for this shift.

Based on the above evidence, it is plausible that the two lines are emitted from the same matter in the dense cores. We can, therefore, combine the results to derive densities in these regions. The main determinant of the density is the ratio of the two line temperatures, as shown by previous CS multi-transition studies (Snell *et al.* 1984). Both CO and NH$_3$ observations show that the kinetic temperature is around 10 K in these dense cores, except in sources B217 and L1696 A where the temperature is 15 K (Benson 1983). We adopted a kinetic temperature of 15 K in B217 and L1696 A and 10 K in all other dense cores. We then used a grid of large velocity gradient (LVG) models and a χ^2 minimization method to derive the density (see Mundy 1984 for details). The results are shown in Table 2.

b) The CS($5 \rightarrow 4$) Observations

Table 3 lists the result of the $J = 5 \rightarrow 4$ observations toward seven sources, with two positive detections and five negative detections. Upper limits are the 3 σ noise in T_R.

The CS($5 \rightarrow 4$) observations (Table 3) put one more constraint on the physical conditions in the dense cores. One straightforward way to apply the $5 \rightarrow 4$ result is to use it with the $3 \rightarrow 2$ and/or $2 \rightarrow 1$ results to get a separate estimate on the density (or its upper limit). In fact, for sources L1489, L1498,

and L1262 A the $5 \rightarrow 4$ observations provide little additional information because the $5 \rightarrow 4$ line temperature predicted from the $2 \rightarrow 1$ and $3 \rightarrow 2$ lines is lower than the rms noise on the observations. For sources TMC 1, L1696 A, and L1174 there were no $2 \rightarrow 1$ observations. In principle we can use the $5 \rightarrow 4$ and $3 \rightarrow 2$ lines to derive a density or an upper limit on the density; but in several sources, the upper limit on density is too high to have any practical meaning (see col. [5] of Table 3).

c) Density

From Tables 2 and 3 we see that the CS lines are tracing densities from 10^4 to 10^6 cm^{-3} except for L1498 where the $3 \rightarrow 2$ and $2 \rightarrow 1$ lines gave a density of 5×10^7 cm^{-3}. Also listed in Table 2 are density uncertainties due to the intensity calibration which is uncertain by about 10%. Aside from the calibration errors at the telescope, there are mainly two factors that affect our density determination, namely the kinetic temperature used in the model and the beam dilution.

For sources other than L1498, the density uncertainty due to calibration is about a factor of 2 (0.3 on the logarithmic scale). The kinetic temperatures are well confined to 10–15 K by NH$_3$ and CO observations, as mentioned before. Our model indicates that by changing the kinetic temperature from 10 K to 15 K, densities determined from the $3 \rightarrow 2$ and $2 \rightarrow 1$ transitions will decrease by 60% and densities from the $5 \rightarrow 4$ and $3 \rightarrow 2$ or $2 \rightarrow 1$ will decrease by a factor of 5. Therefore, the assumed kinetic temperature does not affect much the density determination when the $5 \rightarrow 4$ transition is not involved. The sensitivity of the density determination to the assumed temperature can be understood by the population balance of the upper levels of transitions under consideration. Collisional excitation must be frequent enough to maintain a certain population in the upper levels in order to produce the observed emission. The ratio of the upward to downward collision rate is proportional to e^{-E/kT_k}, where E is the energy difference between the initial and final state of the collisional excitation and T_k is the kinetic temperature. The $J = 5$ state is about 35 K above the ground state and most of the CS molecules are at the $J = 0$–2 states (0–7 K above the ground state) for physical conditions in dense cores. At $T_k = 15$ K, the exponential factor is 3 times bigger than at 10 K, which means the collisional process is 3 times more efficient in populating the upper state. Less frequent collisions, hence lower hydrogen densities are required to populate the upper state. The $J = 2$ and 3 states of CS are only 7 K and 14 K above the ground state; changing T_k from 10 K to 15 K only produces 20%–50% in the exponential factors. This indicates that the density derived from $J = 2 \rightarrow 1$ and $3 \rightarrow 2$ lines should not be very sensitive to temperature.

TABLE 3

RESULTS OF CS($5 \rightarrow 4$) OBSERVATIONS

Source Name (1)	T_R(K) (2)	$J = 5 \rightarrow 4$ ΔV(km s^{-1}) (3)	V (4)	log n(H$_2$) (cm^{-3}) (5)
B5	0.33	0.36	10.3	5.1 ± 0.2
L1489	<0.27	...	...	<7.0
L1498	<0.42	...	...	<8.0
TMC 1	0.21	0.25	5.9	6.0 ± 0.2
L1696 A	<0.48			[a]
L43 B	<0.87			[a]
L1174	<0.48			[a]
L1262 A	<0.54			[a]

[a] The upper limit in density is larger than 10^8 cm^{-3}.
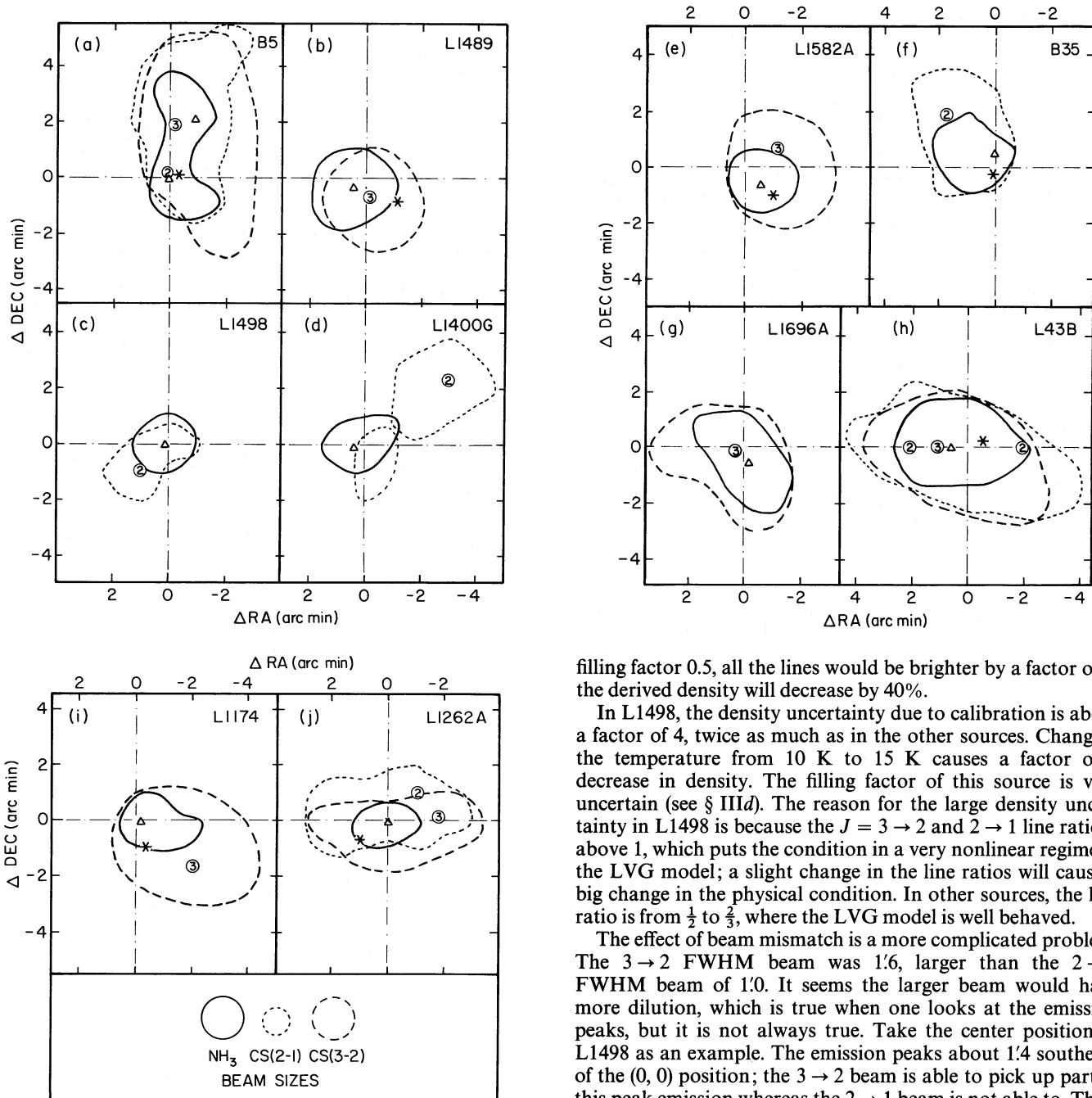
FIG. 3.—The peak positions and the FWHM contours of NH_3 and CS line emission toward 10 sources. The "triangle," "circle 2," and "circle 3" indicate the peak positions of $NH_3(1, 1)$, CS $J = 2 \to 1$, and $3 \to 2$ emissions, respectively. The solid, dotted, and dashed lines are NH_3, CS $J = 2 \to 1$ and $3 \to 2$ contours, respectively. The asterisk indicates the position of associated *IRAS* source except in (e) where it indicates position of a 2 μm source instead. The FWHM beam sizes are at the bottom. All the NH_3 data are taken from Benson (1983).

Beam dilution can be caused by a clumpy structure as well as unmatched beams. The former can change the absolute intensity of lines while maintaining the same line ratio; the latter will change the line ratio. If the cores are clumpy with a volume filling factor of 0.3 (see § IIId) which implies a surface

filling factor 0.5, all the lines would be brighter by a factor of 2; the derived density will decrease by 40%.

In L1498, the density uncertainty due to calibration is about a factor of 4, twice as much as in the other sources. Changing the temperature from 10 K to 15 K causes a factor of 3 decrease in density. The filling factor of this source is very uncertain (see § IIId). The reason for the large density uncertainty in L1498 is because the $J = 3 \to 2$ and $2 \to 1$ line ratio is above 1, which puts the condition in a very nonlinear regime of the LVG model; a slight change in the line ratios will cause a big change in the physical condition. In other sources, the line ratio is from $\frac{1}{2}$ to $\frac{2}{3}$, where the LVG model is well behaved.

The effect of beam mismatch is a more complicated problem. The $3 \to 2$ FWHM beam was $1\rlap{.}'6$, larger than the $2 \to 1$ FWHM beam of $1\rlap{.}'0$. It seems the larger beam would have more dilution, which is true when one looks at the emission peaks, but it is not always true. Take the center position of L1498 as an example. The emission peaks about $1\rlap{.}'4$ southeast of the (0, 0) position; the $3 \to 2$ beam is able to pick up part of this peak emission whereas the $2 \to 1$ beam is not able to. Thus, the ratio of the $3 \to 2$ to $2 \to 1$ emission is overestimated, which might be partially responsible for the high density derived in this source. If we take the beam difference into account for L1498, we can raise the $2 \to 1$ radiation temperature from 0.98 to 1.15 K. In other sources, the beam mismatch can cause an uncertainty of 10% in line ratios, which is comparable to the calibration uncertainty.

In short, for sources other than L1498 the uncertainty in density is about a factor of 4, contributed equally by calibration and beam mismatch. With matched beams, one can hope to reduce the uncertainty to a factor of 2. In L1498, the density is uncertain by an order of magnitude; a different pair of lines from $J = 3 \to 2$ and $2 \to 1$ is needed to trace the density in this source.
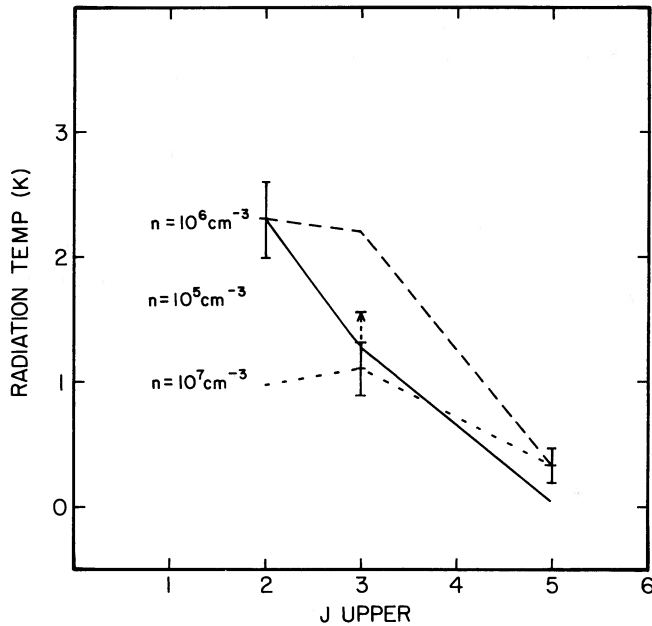
FIG. 4.—The LVG model fits to CS lines in B5 at a constant kinetic temperature of 10 K. The upper dashed line ($n = 10^6$ cm^{-3}) fits well to CS $J = 2 \rightarrow 1$ and $5 \rightarrow 4$ lines; and the lower dashed line ($n = 10^7$ cm^{-3}) fits well to the CS $J = 3 \rightarrow 2$ and $5 \rightarrow 4$. All three lines cannot be fitted simultaneously with a single density model.

B5 is the only source for which we have positive detections in all three lines. As indicated in Table 2, the $2 \rightarrow 1$ and $3 \rightarrow 2$ line pair gives a density estimate of $\sim 4 \times 10^4$ cm^{-3}; the $5 \rightarrow 4$, $3 \rightarrow 2$ and $5 \rightarrow 4$, $2 \rightarrow 1$ pairs give a density estimate of 10^7 cm^{-3} and 10^6 cm^{-3}, respectively. All three lines together give a density estimate of $\sim 10^5$ cm^{-3} (Table 3); this is because the $5 \rightarrow 4$ carries little weight due to its large uncertainty. Figure 4 shows some model fits to the CS lines toward B5. One interesting thing we see is that there is no single model that fits all three lines. In all cases we have assumed an excitation temperature of 10 K, as indicated by NH$_3$ observations (Benson 1983). CO observations toward this source give an excitation temperature of 13 K. Changing the temperature to 15 K does not alter the situation; by considering the beam dilution in $3 \rightarrow 2$, we can raise the radiation temperature to about 1.7 K (dashed arrow in Fig. 4), which makes it closer to the $n = 10^6$

cm^{-3} fit but not quite on the line. Furthermore, if the $5 \rightarrow 4$ emission is not as extended as the lower J emission, the $5 \rightarrow 4$ line would be significantly brighter when corrected for beam dilution, which makes it more difficult to fit all the lines with a single model.

Comparison of the line widths of the three transitions in B5 gives a clear indication that there might be two components of gas present in the source. While the center velocity of the three lines agree, the width of the $5 \rightarrow 4$ transition (0.36 km s^{-1}) is much smaller than the widths of the $3 \rightarrow 2$ and $2 \rightarrow 1$ (0.8 and 0.7 km s^{-1}); the difference is at the 3 σ level of the uncertainty in our estimation. A simple explanation is that one component of the gas has a wider line width (~ 0.7 km s^{-1}) and lower density ($\sim 10^4$ cm^{-3}) and is emitting most of the $2 \rightarrow 1$ and $3 \rightarrow 2$ lines; a second component of gas has a narrower line width (~ 0.3 km s^{-1}) and a higher density ($\sim 10^6$ cm^{-3}) and is contributing most of the $5 \rightarrow 4$ emission. The two components may coexist in different proportions in different cores. For example, in L1498 the gas may be dominated by the second component (the density in this core is at least 10^6 cm^{-3} as discussed before), and in B5 the gas is more of a mixture of the two components. To analyze this situation consistently, a more sophisticated radiative transfer model is needed (e.g., Leung 1975). A more complete discussion of this aspect will be given by Fuller and Myers (1989).

We have also derived densities from the CS($2 \rightarrow 1$) and ($3 \rightarrow 2$) lines over the mapped region in B5, L43 B, and L1262 A. The density is fairly constant across the cores; no significant structure is seen.

d) Mass

Once we have both the size and density estimates, we can derive the mass. Assuming the core size along the line of sight to be the geometric average of the long and short axes (FWHM size in Table 4 corrected for beam size broadening) on the plane of the sky, we estimate the volume of the core to be $(\pi/6)R^3$, where

$$R = D(\theta_{\text{short}} \times \theta_{\text{long}})^{1/2} ,$$

D is the distance to the source (see Table 4). The total mass is the product of volume and the density from either Table 2 or Table 3. The results are listed in Table 4. Note that for L1498, we adopted a density of 2.5×10^6 cm^{-3} (see discussion in § IIIc above).

TABLE 4

SIZES AND MASSES

Source Name	$J = 2 \rightarrow 1$ $\theta_{\text{FWHM}}('')$	$J = 3 \rightarrow 2$ $\theta_{\text{FWHM}}('')$	D (pc)	R (pc)	M ($M_\odot$)	M_{vir} ($M_\odot$)
B5	3.6 × 7.4	4.5 × 8.0	350	0.55	200	65
L1489	2.5 × 4.0	3.0 × 3.5	140	0.12	1.0	9.4
L1498	2.0 × 4.0	...	140	0.11	2000[a]	3.0
L1400 G	2.5 × 6.2					
L1535	4.5 × 5.5					
L1582 A	...	3.5 × 4.0	400	0.40		34
B35	3.0 × 4.7	...	400	0.42		470
L1696 A	...	2.5 × 4.5	160	0.13		13
L43 B	3.3 × 8.5	3.5 × 6.5	160	0.22	64	25
L255	4.7 × 8.7	...	160	0.29	<920	15
L1152	2.1 × 4.1	...	440	0.35		29
L1174	...	3.0 × 5.0	440	0.45		120
L1262 A	2.5 × 5.6	2.5 × 6.0	200	0.20	120	19

[a] This mass is very uncertain since the density is not well determined in L1498.

In the last column of Table 4, we list the virial mass of the cores estimated from the size and velocity width of the CS emission:

$$M_{\rm vir} = 210 \times \frac{R}{\rm pc} \left(\frac{\Delta V_{\rm FWHM}}{{\rm km\ s}^{-1}}\right)^2 M_\odot \ .$$

Here, the velocity width is taken from the spectra at the peak emission, averaged over $J = 3 \to 2$ and $2 \to 1$ lines. If one believes that the virial mass reflects the true mass of the dense cores, the ratio of the virial mass and the mass estimate from density and volume should indicate the volume filling factor of the CS emission (Snell *et al.* 1984). From Table 4, we see that the virial masses of the cores are mostly less than the mass estimate from density and size, which suggests a volume filling factor $f_v \sim 0.2$—0.4. The one exception is L1489, for which the mass estimate from the density and size is less than the virial mass, implying that the core is not virialized.

IV. COMPARISON OF CS AND NH_3 DATA

a) *Size and Shape of Emission Regions*

We first compare the overall size of the CS and NH_3 emission regions. The CS sizes are all from our observations and the NH_3 sizes are measured directly from the contour maps published in Benson (1983), using the same definition of size. As shown in Figure 3, the size of the NH_3 emission region is invariably smaller than that of the CS. The two sizes do correlate; i.e., for cores with more extended NH_3 emission, the CS emission region also tends to be larger. Furthermore, Fuller (1989) and Fuller and Myers (1989) find a significant correlation in position, and a moderate correlation in aspect ratio, for 12 cores mapped in the $NH_3(1, 1)$ line and in the $CS(2 \to 1)$ line.

In general, details of the CS and NH_3 line temperature contour maps do not agree. For instance, in B5 the ammonia map breaks into two clumps while the $CS(2 \to 1)$ and $(3 \to 2)$ maps have only one peak somewhere between the two ammonia peaks (Fig. 3). Overall, among a sample of 10 dense cores for which we have both CS and NH_3 maps, three cores have CS peak positions more than 2′ away from the NH_3 peak positions. In L1400 G, the CS peak position is 3′ away from the NH_3 peak position. In four of the cores, the half-maximum contours of CS maps are noticeably offset those of NH_3 maps by half of the NH_3 map FWHM. We cannot attribute all the differences to pointing and calibration errors in the observations. There must be a significant difference in the distribution of these two molecules in at least a third of the sample.

A possible explanation for some of the differences between the CS and NH_3 data has been noted briefly by Fuller and Myers (1987). If the optical depth measured outward from the half-maximum contour is less than 1 for the NH_3 line but greater than 1 for the CS line, then the FWHM map diameter can be significantly larger for CS than for NH_3, for two reasons: (1) the observed CS emission peak will be weaker than that arising just from the CS in the NH_3 core because of foreground self-absorption, and (2) the CS molecules outside the NH_3 core will scatter some CS line photons from inside the NH_3 core toward the observer. Some evidence that favors this scenario comes from high spectral resolution observations of CS $2 \to 1$ line profiles. These profiles show self-absorption dips which are not evident in the corresponding NH_3 line profiles. These observations and a more quantitative discussion are presented in Fuller (1989) and in Fuller and Myers (1989).
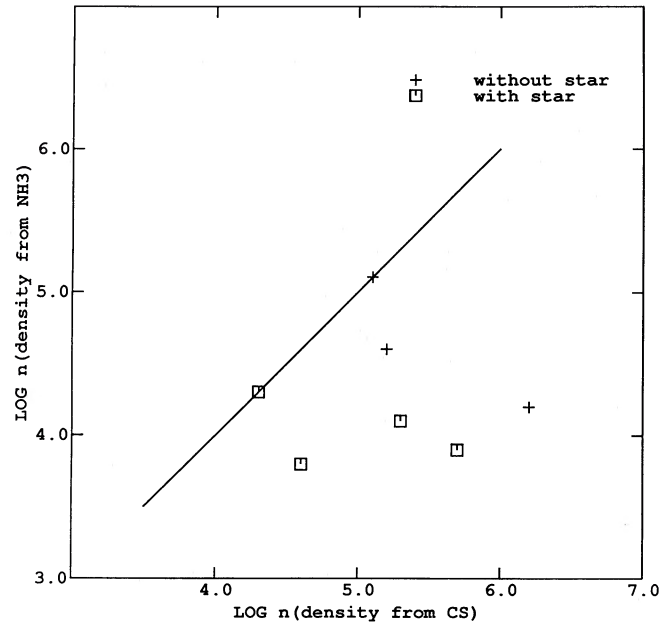
FIG. 5.—The log of the H_2 density derived from excitation analysis of NH_3 is plotted vs. that derived from the CS lines. The two symbols separate sources associated and not associated with *IRAS* point sources.

b) *Density and Mass*

Figure 5 plots the densities estimated from NH_3 versus those determined from CS toward a number of cores. The ammonia density estimates are taken from Benson (1983); the CS densities are taken from Table 2 except for L1498, where we corrected the density for beam dilution. We see that there is no clear correlation between the two. CS is probing densities ranging from 10^4 to 10^6 cm^{-3}, while NH_3 generally indicates $n \sim 10^4$ cm^{-3} (Myers and Benson 1983). The average density from the CS data is about a factor of 10 higher than that from the NH_3. Together with the smaller size of the NH_3 maps and their tendency to center on the infrared sources, this result leads to a very peculiar conclusion: the density appears to *increase* with increasing distance from the forming star, contrary to theoretical expectations. We will discuss some ways to avoid this paradoxical conclusion.

First we note that each transition is sensitive only to a restricted range of densities, usually characterized by the critical density, $n_c = A/\gamma$, where A is the spontaneous emission rate and γ is the collisional rate coefficient. In particular, if $n \gg n_c$, the transition approaches thermalization and only a lower limit to n can be found. The critical density of the NH_3 $(J, K) = (1, 1)$ line is only 2×10^3 cm^{-3}, as opposed to 5.7×10^5 cm^{-3} and 1.5×10^6 cm^{-3} for the CS $J = 2 \to 1$ and $3 \to 2$ lines. The difference in the actual excitation is less extreme than this comparison would indicate because stimulated transitions are much more important at the lower frequency of the NH_3 line (see Evans [1989] for a discussion of this point). To get a better idea of the excitation, we plot $T_{\rm ex}$ versus log n in Figure 6; these are the results of large velocity gradient models for $T_K = 10$ K and column densities appropriate to these sources. While the difference is much less than would be expected from comparing n_c, the NH_3 does thermalize at lower densities than CS.

With these results in mind, we explore the possibility that
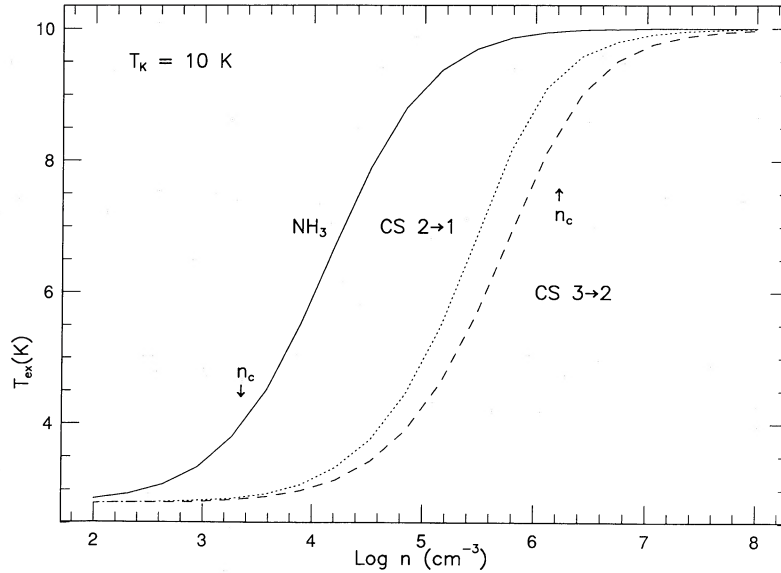
FIG. 6.—Excitation of the $NH_3(1, 1)$, $CS(2 \rightarrow 1)$ and $(3 \rightarrow 2)$ lines vs. density, calculated from LVG models. The assumed column densities of NH_3 and CS are 3×10^{14} and 2×10^{12} cm^{-2}, respectively. The arrows indicate the critical densities.

NH_3 has underestimated the density or that CS has overestimated it. The densities derived from NH_3 [hereafter referred to as $n(NH_3)$] by Benson (1983) were based partially on excitation calculations using collision rates calculated by Green (1981). New collision rates (Danby et al. 1987) have little effect on the density estimates (Gusten and Fiebig 1988). However, Stutzki and Winnewisser (1985) have found that multilevel effects can result in a second solution, with much higher densities. Since their calculations were for $T_K \geq 18$ K, it is not yet clear if this effect is important in these clouds. With regard to CS, we note that different assumptions about the velocity field in the radiative transport can affect $n(CS)$ at the factor of 3 level (more if self-absorption is important), and that similar n_c for the two transitions do not make for a very accurate density probe (see Evans et al. 1987).

Next we consider the uncertainties in the densities from various observational sources. Random noise and calibration uncertainties result in uncertainties in log $n(CS)$ of ± 0.3; $n(NH_3)$ is less affected. A more dramatic effect is that of incomplete beam filling. Because $n(CS)$ and $n(NH_3)$ are derived in very different ways, incomplete beam filling *decreases* $n(CS)$, but *increases* $n(NH_3)$. Plausible filling factors can decrease log $n(CS)$ by about 0.3 and increase log $n(NH_3)$ by about 1.0. For the case of two of the worst discrepancies in Figure 5, we find that log $n(CS) = 5.3$ ($+0.4$, -0.9) and log $n(NH_3) = 4.1$ ($+0.7$, -0.2) for L43 B and log $n(CS) = 5.7$ ($+0.4$, -1.0) versus log $n(NH_3) = 3.9$ ($+1.2$, -0.2) for L1262 A, including all sources of uncertainty that we considered. Thus, $n(NH_3)$ *may* be equal to, or even slightly higher than, $n(CS)$, if filling factors are about 0.5. This possibility can be tested with VLA observations; initial results do not indicate high contrast clumping (Goodman et al. 1989). We conclude that the cause of the apparent inverted density structure is not yet clearly known.

The mass estimates from NH_3 range from 0.1 to 10 $M_\odot$ (Myers and Benson 1983; Benson 1983), and the mass estimate from CS ranges from 1.0 to 200 $M_\odot$. Again, there is no correlation shown between the two, but the CS-based masses are consistently larger because the CS cores have both higher densities and larger sizes than do the NH_3 cores. For both mol-

ecules, the masses were calculated by multiplying the density estimate at the peak position by the volume of the core at the half-maximum contours.

c) Velocity and Velocity Width

The center velocity of the CS and NH_3 lines agree within 0.1 km s^{-1}, but the line widths differ by a factor of 2 or so. Figure 7 and Table 6 show NH_3 line width versus the CS line width. The NH_3 velocity and line widths are from Benson (1983); both were derived from fitting the (1, 1) spectra with all 18 hyperfine components. The CS data are from Table 2; an average value is taken where both $2 \rightarrow 1$ and $3 \rightarrow 2$ data are available. We see that in all the cores, contrary to the naive
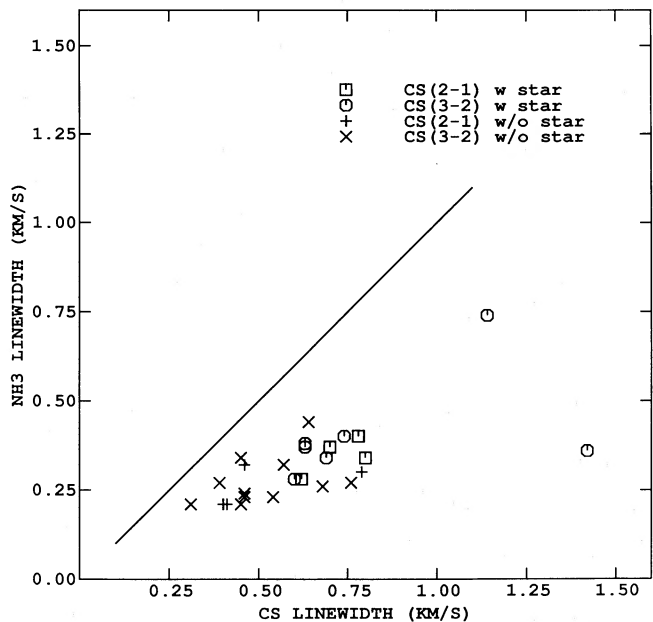
FIG. 7.—Plot of ammonia FWHM line width vs. CS FWHM line width. The straight line shows when the line widths of NH_3 and CS are equal.

prediction of nonthermal broadening with fixed thermal motions, the NH_3 line width is narrower than that of CS. The uncertainty in the line width measurement is less than 0.1 km s^{-1} for CS and less than 0.08 km s^{-1} for NH_3. We will discuss in detail the possible reasons for the line width difference in the following paragraphs.

i) Optical Depth Effects

One thing we did not take into account in our line width comparison is the optical depth effect for the CS line. The NH_3 line widths plotted in Figure 7 are all intrinsic, meaning that broadening due to optical depth has been taken out by using fits to the weaker hyperfine lines, but the CS line widths are determined by fitting Gaussians to the observed spectra.

To estimate the optical depth of the CS lines, we observed the $C^{34}S(3 \to 2)$ transition at MWO toward four sources. All detections were negative, and the rms noise in the spectra is given in Table 5, along with the antenna temperature of the line from the common isotope. Assuming that the abundance ratio of CS and $C^{34}S$ is 20, and that the maximum possible strength for the $C^{34}S(3 \to 2)$ line is twice the rms noise, we can estimate a 2 σ upper limit to the optical depth from the following formula:

$$\tau \leq \frac{20 \times 2 \times T_{A, \text{rms}}{}^*(C^{34}S)}{T_A{}^*(CS)} .$$

Results are listed in column (4) of Table 5.

The line broadening due to optical depth effects is discussed in detail in Phillips et al. (1979). We use equation (3) in their paper, appropriate for a Gaussian line shape:

$$\Delta v = \frac{\Delta v_i}{(\ln 2)^{1/2}} \left[\ln \left\{ \frac{\tau_p}{\ln \left[2/\exp\left(-\tau_p\right) + 1 \right]} \right\} \right]^{1/2} ,$$

where Δv is the observed line width, Δv_i is the intrinsic line width, and τ_p is the optical depth of the line. Here we use the NH_3 line width as the intrinsic line width and predict the required optical depth τ_p to explain the observed CS line width. The results are listed in column (5) of Table 5.

It is certain that in B5 and L1696 A, the line width difference between NH_3 and CS cannot be explained by the optical depth effects, even if we take into account the uncertainty in our line width measurements. On average, the ratio of the CS line width to the NH_3 line width is 2.0 ± 0.6, which requires an average optical depth of 10 to explain the ratio. To determine whether the case of B5 and L1696 A is general to all dense cores will require a sensitive survey of isotopic CS lines.

ii) Turbulent Width versus Cloud Size

A number of authors have discussed the variation of line width with the size of the cloud seen in the same line. Myers

TABLE 5
RESULTS OF $C^{34}S(3 \to 2)$ OBSERVATIONS

Source Name (1)	$C^{34}S(3 \to 2)$ $T_A{}^*$(rms K) (2)	$CS(3 \to 2)$ $T_A{}^*$(K) (3)	τ (max) (4)	$\tau_p{}^a$ (required) (5)
B5	0.03	0.69	1.7	11
L1696 A	0.07	0.70	4.0	100
L43 B	0.14	0.61	9.2	5
L1174	0.07	0.36	7.8	3

^{a} τ_p is the optical depth required if thermal broadening is dominant in CS lines.

(1983), Leung et al. (1982), and Larson (1981) have analyzed clouds with sizes ranging from 0.1 to 100 pc and all concluded that the line width decreases as the cloud size gets smaller, though they differ slightly on how strong the trend is. Since in § IVb above we found that the CS emission region is larger than that of NH_3, it follows that the CS width should be wider than that of NH_3. The question is whether the difference in size is enough to explain the difference in line width, provided the line width–size relationship from previous studies is also applicable here.

We take the $\Delta v \propto R^{0.5}$ relation from Myers (1983) since the sample of clouds used in his study is almost identical to the ones we have here. Note that Δv is the turbulent width, which is related to the intrinsic line width Δv_i is the following way:

$$\Delta v_{\text{turb}} = [(\Delta v_i)^2 - 8(\ln 2)kT_k/m]^{1/2} ,$$

where the second term in the bracket is due to the thermal line broadening. For $T_k = 10$ K, the CS thermal width is 0.10 km s^{-1}, and the NH_3 thermal width is 0.16 km s^{-1}. The derived turbulent widths for both CS and NH_3 are listed in Table 6.

The average ratio of the CS map size to that of NH_3 is 1.5 ± 0.3, so the turbulent width ratio predicted from the size ratio is only 1.2. Since the average ratio of the turbulent widths of the two molecules is 2.3 ± 0.6, there is a factor of ~ 2 which cannot be explained by this argument. If we take into account both the optical depth effect and the size difference of the emission regions, the required average optical depth of the CS lines is still on the order of 10. The basic difficulty remains.

One caution about the line width–size relationship is that the $\Delta v \propto R^{0.5}$ law was defined from cloud to cloud, but not well defined for different parts of the same cloud. An earlier work on different regions of the ρ Oph cloud suggested a $\Delta v \propto R^{0.35}$ law (Myers et al. 1978). This law would have more difficulty in explaining line width difference.

iii) Chemical Differentiation

As discussed in § IVa above, the peak position and the half-maximum contours of the CS and NH_3 emission differ in about a third of the cores. This suggests that at least some of the CS and NH_3 line emission comes from different parts of the clouds. Strong evidence for this comes from the fact that $NH_3(1, 1)$ line requires a lower density to excite than the CS lines and yet it emits in a smaller region. If NH_3 to CS abundance ratio is constant throughout the cloud, one should certainly see NH_3 wherever CS is seen. On the other hand, the CS and NH_3 line velocities are extremely similar: from Table 2 of this paper and Table 1 of Myers and Benson (1983), the distribution of difference in line velocity $V(CS) - V(NH_3)$ for 21 sources has a mean of 0.03 km s^{-1} and a standard deviation of 0.11 km s^{-1}. This comparison suggests that the CS and NH_3 emission volumes have substantial overlap.

One possible scenario is that ammonia is underabundant relative to CS in the presence of supersonic turbulence. The CS line widths are then dominated by emission from regions with supersonic turbulence while the NH_3 line widths are dominated by subsonic turbulence. In addition, CS and NH_3 emissions overlap in the regions with subsonic turbulence, which accounts for the similarity in their line velocity. The separation of CS and NH_3 emission is not peculiar to low-mass cores; it has also been seen in the high-mass star-forming region NGC 2071 (Takano et al. 1986). The problem may be a general one and suggests that a study of what determines the abundances of these two molecules may be interesting.

TABLE 6

SUMMARY OF PROCESSED DATA

SOURCE NAME	ΔV_{turb} (km s^{-1})		Size (pc)		log $n(H_2)$ cm^{-3}	
	CS	NH$_3$	CS	NH$_3$	CS	NH$_3$
Cores Associated with *IRAS* Point Sources						
B5(−1, 1)	0.74	0.30	0.55	0.32	4.6	3.8
L1489(0, −1)	0.60	0.23	0.13	0.07	4.3	4.3
L1535	...	0.66				4.3
TMC 1A	0.78					
L1582 B	1.35					
B35	2.31		0.44	0.19		
L43 B(1, 0)	0.73	0.37	0.23	0.09	5.3	4.1
L255	0.49	...	0.29			
L1152	0.62	0.34	0.37	0.22		
L1174	1.14	0.72	0.50	0.19		
L1172	1.42	0.31				
L1251	1.30					
L1262 A	0.67	0.33	0.22	0.09	5.7	3.9
Cores Not Associated with *IRAS* Point Sources						
L1498	0.35	0.14	0.11	0.06	6.2	4.2
L1495	0.45	0.18				
L1400 G	0.78	0.25	0.19	0.10		
B217	0.43	0.28				
TMC 2	0.75	0.22				
TMC 1	0.56	0.28			6.0	4.1
L1512	0.41	0.14			5.1	5.1
L1582 A	0.63	0.41	0.43	0.17		
L134 A	0.53	0.28			5.2	4.6
L183	0.53	0.17				
L1696 A(0, −1)	0.67	0.17	0.16	0.11		
L1709	0.73					
L234 A	0.45	0.16				
L63	0.38	0.22				

V. DISCUSSION

a) Morphology

We have searched the *IRAS* Point Source Catalog for sources associated with the CS cores. Our criterion for "association" is that the *IRAS* source has to be within the CS half-maximum contour for cores mapped in CS and within a 2' radius for cores not mapped in CS. For the 27 dense cores we observed in CS, 13 are found to have associated *IRAS* point sources. The results are listed in the last column of Table 1. In comparison with the search of Beichman *et al.* (1986), our criterion for "association" is much more strict, and yet the results are about the same.

Figure 3 shows the half-maximum contour of CS and NH$_3$ emission (in $T_A{}^*$) for the cores we mapped in either CS(3 → 2) or (2 → 1). There are six cores associated with infrared point sources (either *IRAS* or 2 μm). For five of these cores, the NH$_3$ contour falls within the CS contours. The emission peaks typically differ by 2', slightly larger than the CS beam width. The stellar position is always in the CS contour, but is just outside the ammonia contour in one case (L1489). There is no general coincidence of the stellar position and the molecular line emission peaks. In the southern part of B5, the infrared source is right on the CS and NH$_3$ emission peaks; but in L1489 the infrared source is outside the NH$_3$ half-maximum contour; and in B35 the stellar position is more than 2' away from the CS emission peak.

For the three cores with no associated infrared sources, the CS emission region differs from the NH$_3$ emission region by

varying degrees. The most pronounced deviation is found in L1400 G, where the CS emission breaks into two parts with the CS emission peak outside the NH$_3$ contour. Even in the northern part of B5 where no infrared source has been found to associate with the northern NH$_3$ emission peak, the CS emission is much more extended than the NH$_3$ emission.

It is possible that this separation of CS and NH$_3$ exists in all cores; the coincidences we see could be due to projection and inadequate spatial resolution. The exploration of projection effects requires a large set of maps of these dense cores in both CS and NH$_3$; high-resolution observations of selected cores seems to be a better way to investigate the problem.

b) Line Widths and Line Width–Size Relationship

When a young star forms in a dense core, it will undoubtedly put energy into the surrounding gas. One expectation is that part of the energy will be turned into kinetic energy of the gas and increase the widths of molecular lines. For the 13 cores with associated *IRAS* sources, the average line width is 0.99 ± 0.13 km s^{-1}; for the 14 cores without associated *IRAS* sources, the average line width is 0.55 ± 0.04 km s^{-1}. Statistical tests show that the former is larger than the latter at the 99% confidence level. The big standard deviation in the line widths of cores with associated *IRAS* sources is mainly attributed to lines that are much wider than the average.

It is well known that the width of NH$_3$ lines is wider for cores with associated *IRAS* sources (Beichman *et al.* 1986; Fuller 1988). The present result shows that the CS and NH$_3$ lines are equally effective in detecting the kinematic changes in
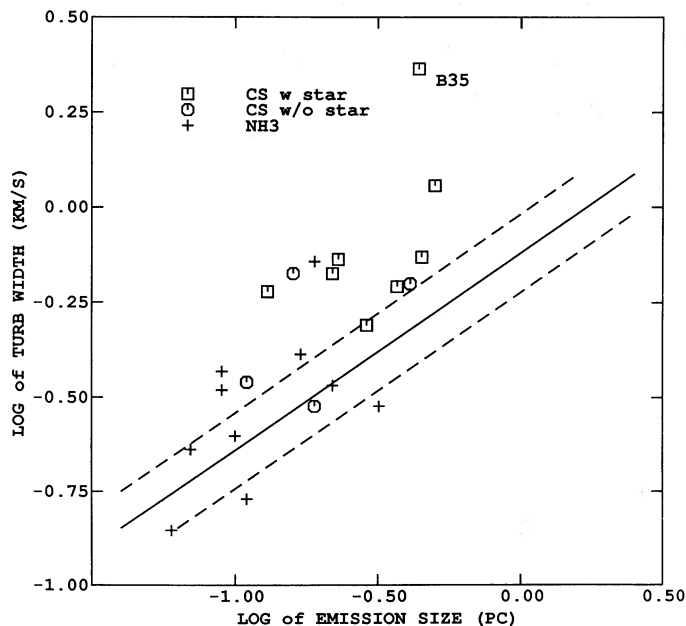
FIG. 8.—Plot of the turbulent width vs. the size of emission region. The solid line is the best fit to NH$_3$ data taken from Myers (1983), and the dashed lines show the 1 σ uncertainty of the best fit.

the cores due to star-formation processes, in spite of their different properties.

As discussed in § IV*c*, the CS lines are wider by a factor of 2 than are the NH$_3$ lines, but the size of the emission regions is only 1.5 times as big. This will put the CS lines above the best-fit line on the line width–size plot from Myers (1983) (Fig. 8). However, this does not necessarily mean that the CS lines do not follow the $\Delta V \propto R^{0.5}$ law. The widest CS line is seen in B35, which is a bright-rimmed cloud possibly being disturbed by ionization-driven shock waves (Lada and Black 1976). If we take the B35 point off Figure 8, the CS line would follow the same power law with a larger coefficient than NH$_3$. There are several studies suggesting that the $\Delta V \propto R^{0.5}$ relationship breaks down on scales somewhere between 0.1 and 1 pc (cf. Falgarone 1989). The breakdown, if it exists, might indicate that some new physical process, different from those seen on larger scales, comes into play. The most notable process is the formation of stars.

c) *Density and Stability of Cores*

Myers and Benson (1983) have analyzed the stability of dense cores in detail using the ammonia lines as tracers. They compare the derived density with the critical density and concluded that all the cores are either close to critical conditions or in their early collapse. In the Doppler motion supported case, the critical density

$$n_{\text{crit}} \propto (\Delta V/R)^2 \ .$$

If we use the CS as the density tracer, ΔV will be greater by a factor of 2 and R larger by a factor of 1.5; overall the critical density will go up by a factor of 2. The density derived from the CS data is about a factor of 10 higher than that from NH$_3$ (see § IV*a*). Thus, one may conclude that most of the cores are very unstable and are collapsing. However, an overall collapse is not guaranteed; the cloud may be undergoing partial collapse and forming fragments. If this is the case, one should be able to see further density structure with higher spatial resolution CS observations. On the other hand, neither CS nor NH$_3$ line data directly indicate collapse motions with any certainty.

VI. SUMMARY AND FUTURE WORK

The CS line observations have revealed physical conditions in dense cores. For gas temperatures around 10 K the derived density ranges from 10^4 to 10^6 cm^{-3}, and there is evidence for a second component of gas with still higher temperature, density or both. Comparison with NH$_3$ observations have produced two interesting puzzles: on average the CS line widths are a factor of 2 wider than the NH$_3$ line widths; and the CS emission regions are larger than the NH$_3$ regions by a factor of 1.5. The shapes of the CS emission are also different from those of the NH$_3$ emission regions in some cores. We have ruled out CS line broadening as due solely to optical depth effects in a Gaussian line in at least two sources. These two puzzles taken together seem to suggest chemical differentiation in these cores, but it is also important to explore other possible explanations.

Our analysis shows that the line widths are wider in cores associated with infrared sources, and there are indications that the separation of CS and NH$_3$ emission regions are more distinct in cores without stars. The observed CS line widths also support the notion that the line width–size relationship breaks down on the scale of dense cores which may indicate some new physical process, most probably star formation, starts to play a role in the overall cloud dynamics.

We believe that better determination of gas density is needed in order to understand the stability of the cores. Since in the dense cores, higher J transitions are extremely weak due to low temperatures, we have to study them with low J transitions. In the case of CS, the $J = 3 \rightarrow 2$ and $1 \rightarrow 0$ seem to be the best pair to study them, as indicated by our LVG models. High-resolution CS $J = 5 \rightarrow 4$ is also needed to investigate the possibility of a denser component of gas as indicated by B5. The line width difference between CS and NH$_3$ lines and the separation of the emission regions should be pursued with high-resolution CS and NH$_3$ observations.

REFERENCES

Beichman, C. A., Myers, P. C., Emerson, J. P., Harris, S., Mathieu, R., Benson, P. J., and Jennings, R. E. 1986, *Ap. J.*, **307**, 337.
Benson, P. J. 1983, Ph.D. thesis, Massachusetts Institute of Technology.
Benson, P. J., and Myers, P. C. 1989, in preparation.
Benson, P. J., Myers, P. C., and Wright, E. L. 1984, *Ap. J. (Letters)*, **279**, L27.
Danby, G., Flower, D. R., Valiron, P., Kochanski, E., Kurdi, L., and Diercksen, G. H. F. 1987, *J. Phys. B.*, **20**, 1039.
Evans, N. J. II. 1989, *Rev. Mexicana Astr. Ap.*, in press.
Evans, N. J. II, Mundy, L. G., Davis, J. H., and Vanden Bout, P. 1987, *Ap. J.*, **312**, 344.

Falgarone, E. 1989, in preparation.
Fuller, G. A. 1988, Ph.D. thesis, University of California at Berkeley.
———. 1989, in preparation.
Fuller, G. A., and Myers, P. C. 1987, *Physical Processes in Interstellar Clouds. Proc. NATO ASI in Germany*, ed. G. E. Morfill and M. Scholer (Dordrecht: Reidel), p. 137.
———. 1989, in preparation.
Goodman, A. A., Benson, P. J., Fuller, G. A., and Myers, P. C. 1989, in preparation.
Green, S. 1981, *NASA Tech Mem.*, No. 83869.

Gusten, R., and Fiebig, D. 1988, *MPI Radio Astronomy Prep. Ser.*, No. 314.
Kutner, M. L., and Ulich, B. L. 1981, *Ap. J.*, **250**, 341.
Lada, C. J., and Black, J. H. 1976, *Ap. J. (Letters)*, **203**, L75.
Larson, R. B. 1981, *M.N.R.A.S.*, **194**, 809.
Leung, C. M. 1975, *J. Quant. Spectros. Rad. Tranf.*, **16**, 559.
Leung, C. M., Kutner, M. L., and Mead, K. N. 1982, *Ap. J.*, **262**, 583.
Mundy, L. G. 1984, Ph.D. thesis, University of Texas.
Myers, P. C. 1983, *Ap. J.*, **270**, 105.
Myers, P. C., and Benson, P. J. 1983, *Ap. J.*, **266**, 309.
Myers, P. C., Linke, R. A., and Benson, P. J. 1983, *Ap. J.*, **264**, 517.
Myers, P. C., Fuller, G. A., Mathieu, R., Beichman, C. A., Benson, P. J., Schild, R. E., and Emerson, J. P. 1987, *Ap. J.*, **319**, 340.

Myers, P. C., Ho, T. P., Schneps, M. H., Chin, G., Pankonin, V., and Winnberg, A. 1978, *Ap. J.*, **220**, 864.
Phillips, T. G., Huggins, P. J., Wannier, P. G., and Scoville, N. Z. 1979, *Ap. J.*, **231**, 720.
Snell, R. L., Mundy, L. G., Goldsmith, P. F., Evans, N. J., and Erickson, N. R. 1984, *Ap. J.*, **276**, 625.
Stutzki, J., and Winnewisser, G. 1985, *Astr. Ap.*, **148**, 252.
Takano, T., Stutzki, J., Fukui, Y., and Winnewisser, G. 1986, *Astr. Ap.*, **167**, 333.
Ungerechts, H., Walmsley, C. M., and Winnewisser, G. 1982, *Astr. Ap.*, **111**, 339.

NEAL J. EVANS II and SHUDONG ZHOU: Department of Astronomy, University of Texas at Austin, Austin, TX   78712

GARY A. FULLER: Department of Astronomy, University of California at Berkeley, Berkeley, CA   94720

PHILIP C. MEYERS: Center for Astrophysics, 60 Garden Street, Cambridge, MA   02138

YUEFANG WU: Department of Geophysics, Beijing University, Beijing, China